J. Fluid Mech. (1999), *vol.* 395, *pp.* 253–270. Printed in the United Kingdom

© 1999 Cambridge University Press

Directional solidification of a binary alloy into a cellular convective flow: localized morphologies

By Y.-J. CHEN AND S. H. DAVIS

Department of Engineering Sciences and Applied Mathematics,
Northwestern University, Evanston, IL 60208, USA

(Received 21 July 1998 and in revised form 5 May 1999)

A steady, two-dimensional cellular convection modifies the morphological instability of a binary alloy that undergoes directional solidification. When the convection wavelength is far longer than that of the morphological cells, the behaviour of the moving front is described by a slow, spatial–temporal dynamics obtained through a multiple-scale analysis. The resulting system has a parametric-excitation structure in space, with complex parameters characterizing the interactions between flow, solute diffusion, and rejection. The convection in general stabilizes two-dimensional disturbances, but destabilizes three-dimensional disturbances. When the flow is weak, the morphological instability is incommensurate with the flow wavelength, but as the flow gets stronger, the instability becomes quantized and forced to fit into the flow box. At large flow strength the instability is localized, confined in narrow envelopes. In this case the solutions are discrete eigenstates in an unbounded space. Their stability boundaries and asymptotics are obtained by a WKB analysis. The weakly nonlinear interaction is delivered through the Lyapunov–Schmidt method.

1. Introduction

In the absence of flow, the morphological instability of a binary alloy undergoing directional solidification is driven by the adverse gradient of solute concentration at the solid–liquid interface. This instability occurs when the interface advances with a speed V greater than a critical value V_c, when cellular patterns form on the moving front. When the liquid (melt) is flowing, the solute concentration profile is altered. In general, the liquid motions may delay or promote the instability, depending on the interactions between the solute and momentum transport.

Flow-modified morphological instability has been studied by many authors (e.g. see Davis 1993 for a review). Flows can be inherent to the solidifying process, such as solutal convection in a density-stratified melt (Coriell *et al.* 1980; Coriell & McFadden 1989). The motion here is due to buoyancy effects that exist even when the interface is not deformable. Flows can also be imposed through far-field forcing. Examples include plane Couette flow (Coriell, McFadden & Boisvert 1984), an asymptotic suction profile (Forth & Wheeler 1989; Hobbs & Metzener 1991; Schulze & Davis 1994), and stagnation-point flow (Brattkus & Davis 1988).

In the present analysis we examine the morphological instability of a front propagating into a pre-existing cellular convective flow (see figure 1). Such flows exist when thermal or hydrodynamic instabilities occur before the morphological instability, or when the liquid is subjected to a high-frequency vibration or acceleration (g-jitter). The flow is considered to be spatially periodic, with a wavelength $2\pi/\hat{\alpha}$ typically

https://doi.org/10.1017/S0022112099005856 Published online by Cambridge University Press

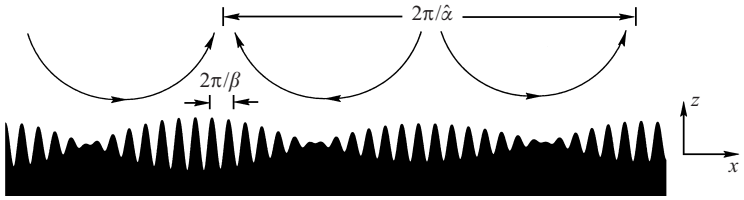


FIGURE 1. Schematic diagram for a spatially periodic flow imposed on the solid–liquid interface of a binary alloy.

much longer than the wavelength $2\pi/\beta$ of the intrinsic morphological instability. This assumption is appropriate for metallic alloys for which typical Schmidt numbers are large, and the viscous lengthscale can be ten or a hundred times longer than the diffusion lengthscale. The present work is related to that of Bühler & Davis (1998), in which numerical calculations of the two-dimensional linear problem have been performed. Their study showed that in such flows the morphological instability can be confined in localized envelopes, distributed spatially periodically along the interface. Each envelope contains many morphological cells travelling in the flow direction. The stability and mechanism of the onset of this solution have yet to be revealed. We extend their analysis and perform stability analysis in the linear and weakly nonlinear regimes. The disturbance is allowed to be three-dimensional, in contrast to the two-dimensional morphology studied in Bühler & Davis (1998).

We treat the solutal–momentum transport as a perturbation of the Mullins–Sekerka problem (Mullins & Sekerka 1964). The 'pure' (no-flow) morphological instability has its critical wavenumber β_c at a critical morphological number M_c, as shown schematically in figure 2(*a*). For $\hat{\alpha}$ small compared with β_c, we use a multiple-scale analysis near the linear-theory critical point (β_c, M_c). The resulting dynamics has a 'parametric-excitation' form in the slow spatial variable, where the periodic coefficients are generated by the cellular flow. The eigenvalue problem of the linearized equation is solved by the numerical branch-tracing technique, with the asymptotics obtained through a WKB-type analysis. Problems of a similar structure have occurred in a number of areas of chemical physics such as molecular spectroscopy and the band theory of solids (see Connor *et al.* 1984), and in the Bénard convection problem with a slow spatial variation of the thermal forcing (Pal & Kelly 1979; Walton 1982). Here, we study the situation of directional solidification coupled with convection.

We observe that disturbances (rolls) periodic in the flow direction (figure 2*b*) are stabilized. The tangential component of the flow either compresses or stretches the morphological cells along the interface, which alters the wave structure and pushes the disturbances to the regime where the surface tension or solute diffusion helps to stabilize them. In contrast, the normal component of the flow has a strong tendency to destabilize rolls parallel to the flow (figure 2*d*). In both cases, the morphologies have incommensurable structures (aperiodic in space) when the flow is weak, and develop localized wave envelopes, as observed in the two-dimensional case in Bühler & Davis (1998), when the flow strength increases. The stability boundary and onset of the travelling cells are identified. Nonlinear interactions of the branching solutions are also discussed.

This paper is organized as follows. Sections 2 and 3 provide the background to the flow-modified morphological problem. We assume that the spatial scale and amplitude

https://doi.org/10.1017/S0022112099005856 Published online by Cambridge University Press

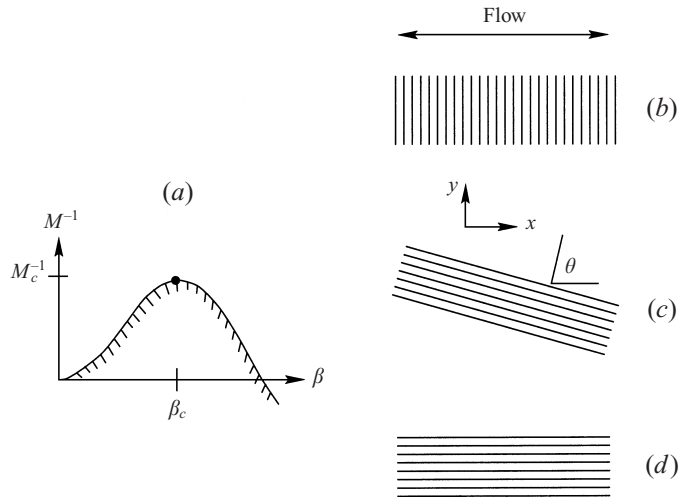


FIGURE 2. (*a*) Neutral stability curve for the pure (no-flow) morphological problem. Solutions in the hatched area are unstable. The morphological cell has a wave vector (*b*) parallel, (*c*) at an angle θ, and (*d*) perpendicular to the flow direction. Series of parallel lines indicate fronts of the cells.

of the flow, and not its details, are important for the morphological instability. Thus, it is possible to introduce a model cellular convection that is driven by an assumed body force. In § 4 we outline the procedures of obtaining the slow-variable equations for roll-like disturbances. Competition between the effects of tangential- and normal-flow components are controlled by the angle θ between the rolls and flow direction. The linear stability analysis is given in § 5. Possible localized, two-dimensional and three-dimensional morphologies are obtained. In § 6 we demonstrate that the localization is realizable in a weakly nonlinear regime. The paper closes with a summary and brief discussion.

2. Solutal transport equations

Consider a dilute binary alloy solidifying into a cellular flow field. The averaged solid–liquid interface moves with a constant velocity V. The solute rejected on the interface has a partition coefficient k and diffusivity D in the liquid. We invoke the 'frozen temperature approximation' (Langer 1980) that gives the temperature T in the solid and liquid permanently by $T = T_0 + Gz$, where G is the imposed temperature gradient and T_0 is a reference temperature. The temperature will not be disturbed when the thermal boundary layer is far thicker than both momentum and concentration boundary layers. The coordinate variable z is fixed on the moving front with positive z-direction pointing into the liquid. The interfacial coordinates are spanned by the (x, y)-axes.

We choose the velocity, time, length, and concentration scales to be V, D/V^2, $\ell_c \equiv D/V$, and $\Delta c \equiv (1/k - 1)c_\infty$, respectively. Referred to these scalings and the chosen coordinates, the solutal transport equation in the liquid can be written

$$\left.\begin{aligned} Sc^{-1}[\partial_t \boldsymbol{v} + (\boldsymbol{v} - \hat{\boldsymbol{e}}_z)\cdot\nabla\boldsymbol{v}] &= -\nabla p + \nabla^2\boldsymbol{v} + \boldsymbol{B}, \\ \nabla\cdot\boldsymbol{v} = 0, \quad \partial_t c + (\boldsymbol{v} - \hat{\boldsymbol{e}}_z)\cdot\nabla c &= \nabla^2 c. \end{aligned}\right\} \tag{2.1}$$

In the above formulation we have assumed the melt to be an incompressible, New-

https://doi.org/10.1017/S0022112099005856 Published online by Cambridge University Press

tonian liquid. The Schmidt number Sc is the ratio of the kinematic viscosity of the liquid to the solute diffusivity. The buoyancy field $\boldsymbol{B}$ is $2\pi/\hat{\alpha}$-periodic in x and is the driving force of the convective flow.

It is assumed that the density change upon solidification is negligible, so that the condition $\boldsymbol{v} = \boldsymbol{0}$ is applied on the solid–liquid interface $z = H(x, y, t)$, and the velocity $\boldsymbol{v}$ approaches the far-field distribution $\boldsymbol{v}_\infty$ as $z \to \infty$. The solute boundary conditions on the interface consist of mass conservation and local thermodynamic equilibrium:

$$v_n[(1-k)c + k] = -\hat{\boldsymbol{n}} \cdot \nabla c \tag{2.2}$$

$$M^{-1}H = 1 - c + \Gamma K(H). \tag{2.3}$$

Here, $\hat{\boldsymbol{n}}$ is the unit normal vector pointing into the liquid phase, v_n the speed of the front normal to itself, and K the curvature, a functional of the interface shape function: $K(H) = \nabla \cdot [\nabla H \{1 + (\nabla H)^2\}^{-1/2}]$. The mass conservation law (2.2) assumes that solute diffusion in the solid is negligible compared with that in the liquid. The Gibbs–Thomson condition (2.3) depicts the departure of the temperature of the interface from the equilibrium melting temperature of the pure solvent due to the presence of solute (constitutional undercooling) and the curvature of the interface itself (capillary undercooling). The morphological number and surface energy parameter are given by

$$M \equiv \frac{\tilde{m} G_c}{G}, \qquad \Gamma \equiv \frac{T_m \gamma}{\tilde{m} G_c \ell_c^2 L_v},$$

where $G_c \equiv -\Delta c/\ell_c$ measures the concentration gradient. The liquidus slope of the phase diagram is denoted by $\tilde{m}$, and the parameters γ, T_m, L_v stand for surface tension, solvent melting temperature, and latent heat per unit volume, respectively.

When $\boldsymbol{B} \equiv 0$ the above system has a solution $(\boldsymbol{v}, H, c) = (\boldsymbol{0}, 0, \mathrm{e}^{-z})$. Consider the stability of this (quiescent) solution to normal-mode perturbations $\mathrm{e}^{\mathrm{i}\boldsymbol{\beta}\cdot(x,y)+\sigma t}$. Linear stability analysis (Mullins & Sekerka 1964) results in the neutral stability curve ($\sigma = 0$), given by

$$M^{-1} = 1 - \Gamma\beta^2 - \frac{k}{k + q - 1},$$

where $q \equiv \frac{1}{2}[1 + (1 + 4\beta^2)^{1/2}]$, and solutions within the curve are unstable ($\sigma > 0$; see figure 2*a*). This neutral curve has a maximum at M_c^{-1} for a critical wavenumber β_c that determines the cellular structure near the onset of the instability. Figure 3(*a*) shows the locus of the critical points (the marginal stability curve) in a pair of transformed coordinates, in which $(M_c\Gamma)^{1/2}$ is proportional to V and independent of c_∞, and the reverse is true for $(M_c/\Gamma)^{1/2}$. The plot shows the relationship between the critical pulling speed V_c and the far-field concentration c_∞ when other physical properties are fixed, and is more appropriate for comparison with experimental observations. For a binary alloy in directional solidification, it is convenient to have constant physical properties and let the pulling speed V vary. When an experiment is operated at a speed V that is inside the unstable region of the marginal stability curve, a cellular pattern forms. The location where a vertical line of constant c_∞ intercepts the lower marginal curve determines the critical pulling speed V_c (figure 3*a*).

3. Basic state

The given cellular flow has a spatial period $2\pi/\hat{\alpha}$, which is considered to be much longer than the morphological lengthscale $2\pi/\beta_c$. The velocity field is represented

https://doi.org/10.1017/S0022112099005856 Published online by Cambridge University Press

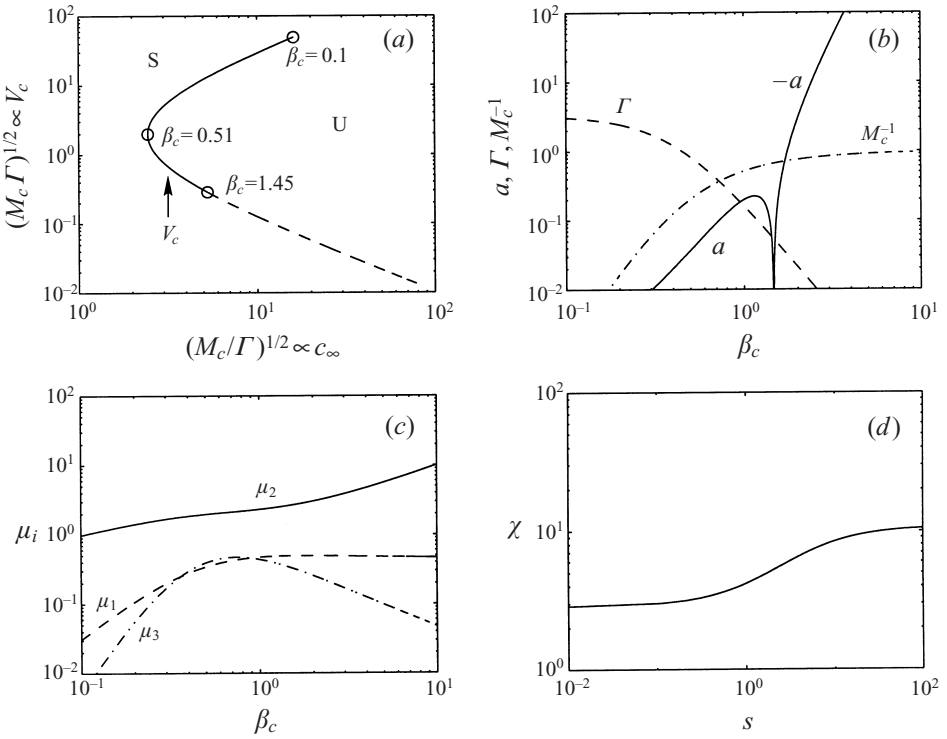


FIGURE 3. (*a*) Marginal stability curve for the pure morphological problem with $k = 0.3$. S denotes stable and U denotes unstable regions. Solid (dashed) line represents supercritical (subcritical) bifurcation. The arrow indicates a path reaching the critical pulling speed V_c for a given c_∞. (*b*) Coefficients (a, Γ, M_c^{-1}) along the marginal stability curve. (*c*) Scaling coefficients (μ_1, μ_2, μ_3) in the flow-modified problem. Values are obtained with an additional flow parameter $s = 1$. (*d*) χ plotted against s when $\beta_c = 0.58$.

by a simple sinusoidal function in the direction x, and exponential in z. We use P to denote the magnitude of the far-field velocity, and consider the case when the tangential component has the form

$$u = -[1 - \mathrm{e}^{-z/s}]P \sin \hat{\alpha} x \tag{3.1}$$

as the interface is flat. This flow has diverging [converging] stagnation points at $(2n+1)\pi/\hat{\alpha}$ $[2n\pi/\hat{\alpha}]$. The parameter s distinguishes a general class of flows. As discussed by Bühler & Davis (1998), its magnitude represents the thickness of the viscous boundary layer near the interface. Flow type (3.1) is motivated by the 'asymptotic suction profile', in which the remote field, $-P \sin \hat{\alpha} x$, is replaced by a constant, and the parameter s is equivalent to the Schmidt number Sc. The asymptotic suction profile is an exact solution to the momentum equation, whereas the remote flow (3.1) here serves as an approximation for flows near the interface. This enables us to simplify the analysis and consider only the situation of large-Schmidt-number metallic alloys ($Sc \to \infty$). Consequently, the liquid inertia is neglected, and the parameter s can take any positive value ($0 < s < \infty$).

Flows with $s \leqslant 1$ can occur in a Hele-Shaw-like apparatus for example, where the close proximity of the sidewalls creates a thin viscous boundary layer. Boundary layers of exponential type are also observed in electrically conducting liquid with flows induced by strong magnetic fields. For those examples the spatial period $2\pi/\hat{\alpha}$

https://doi.org/10.1017/S0022112099005856 Published online by Cambridge University Press

can be introduced through solutal buoyancy or magnetohydrodynamic instability. Accordingly, the body force $\boldsymbol{B}$ in the momentum transport equation would correspond to buoyancy force or Lorentz force, respectively.

We restrict our attention to the case when the basic flow is two-dimensional, but accept three-dimensional disturbances. The velocity field can be expressed in terms of the stream function as $\bar{\boldsymbol{v}} = \boldsymbol{\nabla} \times (\bar{\psi}\hat{\boldsymbol{e}}_y)$. In this formulation the velocity has components $(\bar{u}, \bar{w})$ in the (x, z) directions. We further introduce a coordinate transformation

$$\zeta = \mathrm{e}^{H-z}$$

which maps the interface position $z = H$ to $\zeta = 1$ and the far field $z \to \infty$ to $\zeta \to 0$. The transformation is particularly suitable for nonlinear analysis that requires calculations of higher-order expansions. In this 'Lagrangian' coordinate the stream function with velocity component given by (3.1) is now written

$$\bar{\psi}(x, \zeta) = -[s + \ln \zeta - s\zeta^{1/s}]P \sin \hat{\alpha}x. \tag{3.2}$$

We shall consider (3.2) as the basic-state flow.

When the flow field is treated as an approximate solution to the momentum transport equation, the resulting solutal and interfacial profiles $(\bar{c}, \bar{H})$ can be obtained asymptotically by introducing the expansions

$$\left.\begin{aligned} \bar{c}(\hat{\alpha}x, \zeta) &\sim \zeta + \hat{\alpha}\hat{\delta}\bar{c}_1(\zeta)\cos \hat{\alpha}x, \\ \bar{H}(\hat{\alpha}x) &\sim 0 + \hat{\alpha}\hat{\delta}\bar{H}_1 \cos \hat{\alpha}x, \end{aligned}\right\} \tag{3.3}$$

into the solutal transport equation and boundary conditions. Here, we have scaled the flow by

$$\hat{\delta} \equiv P/(1 + s),$$

and employed a expansion parameter $\hat{\alpha}\hat{\delta}$ to indicate the order of magnitude of the flow perturbation. The perturbations $\bar{c}_1$ and $\bar{H}_1$ are obtained by solving the equations (1)–(3) at $O(\hat{\alpha}\hat{\delta})$ (see Bühler & Davis 1998), which gives

$$\left.\begin{aligned} \bar{c}_1 = \zeta[1/k + (s^2 - 1)\ln \zeta + \tfrac{1}{2}(s + 1)\ln^2 \zeta + s^3(1 - \zeta^{1/s})], \\ \bar{H}_1 = -1/(kM^{-1}). \end{aligned}\right\} \tag{3.4}$$

The expansion (3.3) uses the fact that the solutal and interfacial shape functions are weakly perturbed from the profiles of the quiescent case as $\hat{\alpha}\hat{\delta} \ll 1$. The parameter $\hat{\delta}$ represents the magnitude of the velocity near the interface when $s \ll 1$, and the velocity gradient when $s \gg 1$. This scaling is introduced in the expansions, since only the magnitude of the flow is important when the concentration boundary layer is subjected to an extremely thin viscous layer, while for a thick viscous layer only the velocity gradient near the interface is relevant to the convective transport.

4. Dynamics in slow variables

The imposed flow field breaks the rotational symmetry of the crystal surface. We shall subject the basic state (3.2), (3.3) to a 'roll-like' disturbance, with an angle θ to the flow direction (cf. figure 2*c*). Recall that, in the absence of flow, the most dangerous perturbation is the normal mode $\mathrm{e}^{\mathrm{i}\boldsymbol{\beta}_c \cdot (x,y)}$ at the critical morphological number M_c. In the case of a weak flow (small $\hat{\delta}$) the motion introduces a slow spatial

https://doi.org/10.1017/S0022112099005856 Published online by Cambridge University Press

change. It is thus reasonable to assume that the most dangerous disturbance now has a form $f(\epsilon x)\,\mathrm{e}^{\mathrm{i}\boldsymbol{\beta}_c\cdot(x,y)}$, $0<\epsilon\ll 1$, where $f(\epsilon x)$ is a slowly varying function in the x-coordinate. The parameter ϵ enables us to perform a multiple-scale analysis near the point (β_c, M_c) (see figure 2).

Formally, we assume a perturbation expansion:

$$M^{-1}=M_c^{-1}-\mu_1\epsilon^2 m,\quad \hat{\delta}=\mu_2\epsilon^2\delta,$$
$$\tau=\mu_3\epsilon^2 t,\quad \eta_i=\epsilon^i\beta_c x,\quad \hat{\alpha}/\beta_c=\epsilon\alpha,$$
$$\boldsymbol{u}\sim\bar{\boldsymbol{u}}+\{\epsilon\boldsymbol{u}_1(\tau,\eta_i,\zeta)+\epsilon^2\boldsymbol{u}_2+\epsilon^3\boldsymbol{u}_3\}\,\mathrm{e}^{\mathrm{i}\boldsymbol{\beta}_c\cdot(x,y)}+\{\text{c.c.}\},$$

where $\boldsymbol{u}=(c,H,\boldsymbol{v})$, c.c. represents complex conjugate, and μ_i are real-valued, positive coefficients which will be determined later. By substituting the above expansions into the governing transport equations, and collecting like powers of ϵ, we arrive at a series of linear problems, which can be written as

$$\begin{aligned}
\mathrm{L}\boldsymbol{u}_1&=0, &&O(\epsilon),\\
\mathrm{L}\boldsymbol{u}_2&=F_2(\boldsymbol{u}_1), &&O(\epsilon^2),\\
\mathrm{L}\boldsymbol{u}_3&=F_3(\boldsymbol{u}_1,\boldsymbol{u}_2), &&O(\epsilon^3),
\end{aligned}$$

where L is the linear operator of the no-flow case. Since the operator L is singular, the solvability condition is necessary to solve $\boldsymbol{u}_i$ at each order. The quadratic nature of the turning point at (β_c, M_c) results in the inhomogeneous term $F_2(\boldsymbol{u}_1)$ that is already in the range of L. The leading-order behaviour of H_1 is then determined by the solvability condition at $O(\epsilon^3)$. This procedure results in a dynamical system in the slow variable (dropping subscript '1'):

$$\partial_\tau H=[m+\mathrm{i}\,\delta\cos\theta\sin\alpha\eta]H+\cos^2\theta\,\partial_\eta^2 H-aH|H|^2$$
$$+O(\epsilon\alpha\delta\cos\alpha\eta\,H,\ \epsilon\delta\sin\alpha\eta\,\partial_\eta H). \qquad (4.1)$$

The Landau constant a determines the supercriticality ($a>0$) or subcriticality ($a<0$) of the system. This calculation is performed using a symbolic computation software and the resulting coefficients are listed in table 1 (see also figure 3 for coefficients of selected parameters). When $\delta\equiv 0$, equation (4.1) recovers the Landau equation of the pure morphological problem in Wollkind & Segel (1970). Equation (4.1) is written in the form for which the morphological instability has an $O(1)$ wavenumber in the remote-flow direction ($\cos\theta\approx 1$; cf. figure 2*b*). In this case the tangential-flow component, $\delta\sin\alpha\eta$, is dominant, and the normal component, $\alpha\delta\cos\alpha\eta$, is formally $O(\epsilon)$.

It can be seen from (4.1) that the tangential-flow contribution (proportional to $\cos\theta$) becomes weaker as θ increases (cf. figure 2*b* and figure 2*c*). When θ approaches $\pi/2$, i.e. when the wavevector $\boldsymbol{\beta_c}$ is perpendicular to the flow direction (figure 2*d*), the tangential and normal components of the flow will have the same order of magnitude, $O(\epsilon)$ in equation (4.1); the slow-variable dynamics must then be modified. In this regime we rescale the flow parameter $\delta^*=\epsilon\delta$ such that the flow interacts with the morphological instability at $O(\epsilon^3)$, and redo the multiple-scale analysis. The resulting slow-variable dynamics is governed by

$$\partial_\tau H=[m+\chi\alpha\delta^*\cos\alpha\eta]H+\delta^*\sin\alpha\eta\,\partial_\eta H-aH|H|^2-\tfrac{1}{4}\epsilon^2\partial_\eta^4 H. \qquad (4.2)$$

The fourth-order derivative appears at the higher order of ϵ. Here, the coefficient $\chi=\chi(k,\Gamma,s)$ is a parameter (see table 1) that characterizes the strength of the normal

https://doi.org/10.1017/S0022112099005856 Published online by Cambridge University Press

$$\mu_1 = 4\Gamma(k+3q-2)\beta_c^4/[(2q-1)^2(k+q-1)].$$

$$\mu_2 = 4\Gamma(k+3q-2)\beta_c^4/[(2q-1)^2\varphi\beta_c].$$

$$\mu_3 = 4\Gamma(k+3q-2)\beta_c^4/[(2q-1)^2\{1-\Gamma(k+q-1)\}].$$

$$\chi = 1 + [\Gamma(k+q-1)(1+s)(q-1)/\{(2q-1)[s(2q-1)+1]\} + (1/k-1)(q-1)]/\varphi.$$

$$\varphi = \Gamma(k+q-1)(1+s)/[s(1-2q)-1] + s(1+s)[s(1-q)+1]/[(1-s^2\beta_c^2)^2 \times\{s^2q(q-1)-(1+s)\}] + \beta_c(1+s)(s^3\beta_c^3-2s\beta_c+1)/[(1-s^2\beta_c^2)^2\{(2\beta_c+1) \times(\beta_c+1-q)/\beta_c^2-1/\beta_c\}] + (1+s)(\beta_c+1-q)/[\beta_c(1-s^2\beta_c^2)^2].$$

TABLE 1. Coefficients in the slow-variable equations. The Landau constant a can be found in Wollkind & Segel (1970).

component of the convection relative to that of the tangential component. In our cellular flow setting this parameter is a monotone-increasing function of s and is always greater than unity (figure 3*d*), which implies that a thicker viscous boundary layer (larger s) will induce a stronger contribution from the flow-normal component (larger χ) to the cellular morphology.

Alternatively, one can stretch the spatial coordinate $x \to \epsilon^{1/2}x$ in the primitive equations (Newell & Whitehead 1969) and bring the fourth-derivative term into the $O(\epsilon^3)$ equation. This rescaling, however, is equivalent to a change of the slow variable: $\eta \to \epsilon^{1/2}\eta$, with a pair of redefined (α, δ^*). Therefore, without loss of generality, the system is governed by (4.2); the surface-tension term $\partial_\eta^4 H$ acts as a regularization.

5. Linear stability analysis

To determine the initial behaviour of small disturbances we neglect the nonlinear terms in (4.1), (4.2). It is convenient in the analysis to study only the normal mode: $H(\tau,\eta) \mapsto \mathrm{e}^{(\sigma+\mathrm{i}\omega)\tau}H(\eta)$, and have the disturbance wave vector orientated towards either the x- or y-axis (cf. figure 2*b*, *d*). The resulting system is then referred to as 'two-dimensional' (2D) and 'longitudinal' (3D) rolls respectively, according to its morphological structure:

$$\text{2D-roll:}\ \frac{\mathrm{d}^2H}{\mathrm{d}\eta^2} + [(m-\sigma) - \mathrm{i}\,\omega + \mathrm{i}\,\delta\sin\alpha\eta]H = 0, \tag{5.1}$$

$$\text{longitudinal-roll:}\ -\frac{\epsilon^2}{4}\frac{\mathrm{d}^4H}{\mathrm{d}\eta^4} + \delta^*\sin\alpha\eta\,\frac{\mathrm{d}H}{\mathrm{d}\eta} + [(m-\sigma) - \mathrm{i}\,\omega + \chi\alpha\delta^*\cos\alpha\eta]H = 0. \tag{5.2}$$

The two systems have parametric-excitation forms, driven by the imposed flow. In analogy to a pendulum problem, the 2D-roll equation describes the motion of a 'spatial pendulum' that has a periodic spring constant in accordance with the flow period, and is controlled by complex parameters. The longitudinal-roll equation, as noted, is a singular perturbation problem. The term $\mathrm{d}^4H/\mathrm{d}\eta^4$ is retained since it acts non-uniformly in space.

Floquet theory describes the complicated nature of the spatial behaviour (e.g. see McLachlan 1947, and Mulholland & Goldstein 1929 for complex coefficients). The

https://doi.org/10.1017/S0022112099005856 Published online by Cambridge University Press

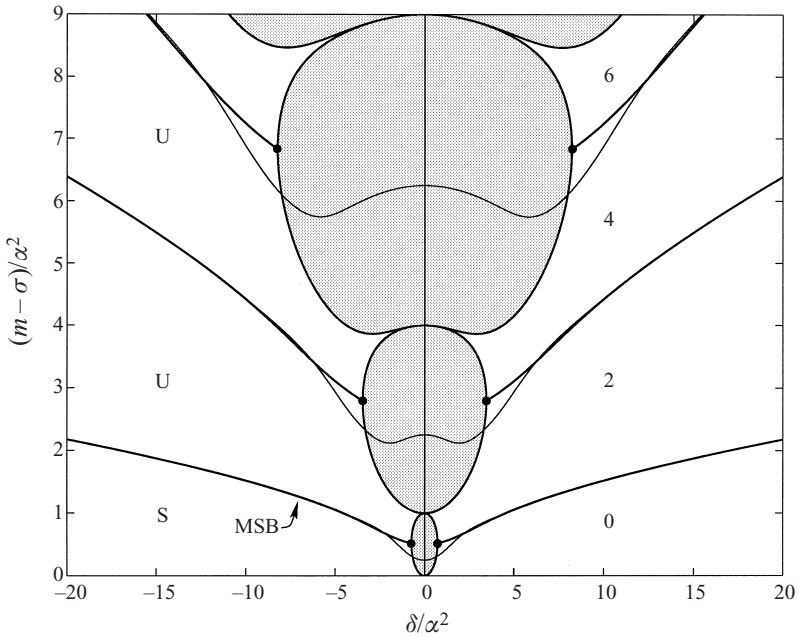


FIGURE 4. Characteristic curves for the 2D-roll equation. Thick lines are period-$(2\pi/\alpha)$ (harmonic) solutions and thin lines are period-$(4\pi/\alpha)$ (subharmonic) solutions. Solutions in the shaded area have spatial structures incommensurate with the flow period. Solid circles represent doubly degenerate points. S denotes stable, U denotes unstable regions. MSB denotes marginal stability boundary.

coefficients have period $2\pi/\alpha$, and there are solutions in the form

$$H(\eta) = \mathrm{e}^{\Lambda\eta}\Phi(\eta), \quad \Phi(\eta + 2\pi/\alpha) = \Phi(\eta),$$

where Λ is the Floquet exponent. Since we are concerned only with the spatially bounded solutions (eigenfunctions), this demands $\mathrm{Re}\,\Lambda = 0$. Figures 4 and 5 show the characteristic boundaries of these solutions, in which the lines were obtained by the numerical branch-tracing technique (Doedel 1981), and numbers indicate the number of modes that have lengths fitted into the flow box. The branching solutions were traced in $[\delta/\alpha^2, (m-\sigma)/\alpha^2, \omega/\alpha^2]$ parametric space for the 2D-roll equation, and $[\delta^*/(\alpha^3\epsilon^2), (m-\sigma)/(\alpha^4\epsilon^2), \omega/(\alpha^4\epsilon^2)]$ space for the longitudinal-roll equation with a selected $\chi > 1$. The parameters listed above represent appropriate scalings when α is small.

In figures 4 and 5 we plot the characteristic curves of the $(2\pi/\alpha)$-periodic (harmonic) and $(4\pi/\alpha)$-periodic (subharmonic) solutions. Solutions within the characteristic boundaries are aperiodic functions, and the interfacial perturbations $H(\eta)$ are incommensurate (spatially unsynchronized) with the flow. These 'incommensurate bands' are shaded in the figures. For the 2D-roll equation, all subharmonic solutions (thin lines in the figure) are oscillatory ($\omega \neq 0$). The harmonic solutions (thick lines) are stationary ($\omega = 0$) when δ/α^2 is small, but change to time-dependent solutions at the doubly degenerate points where branches of solutions cross and pairs of oscillatory modes ($\omega = \pm\omega^*$) bifurcate. In contrast, all solutions of the longitudinal roll are stationary (figure 5), with the incommensurate bands shrinking to thin, film-like layers as $\delta^*/(\alpha^3\epsilon^2) \gg 1$. This behaviour suggests that the eigenstates are essentially quantized. That is, discrete eigenmodes exist in an unbounded state, and the induced

https://doi.org/10.1017/S0022112099005856 Published online by Cambridge University Press

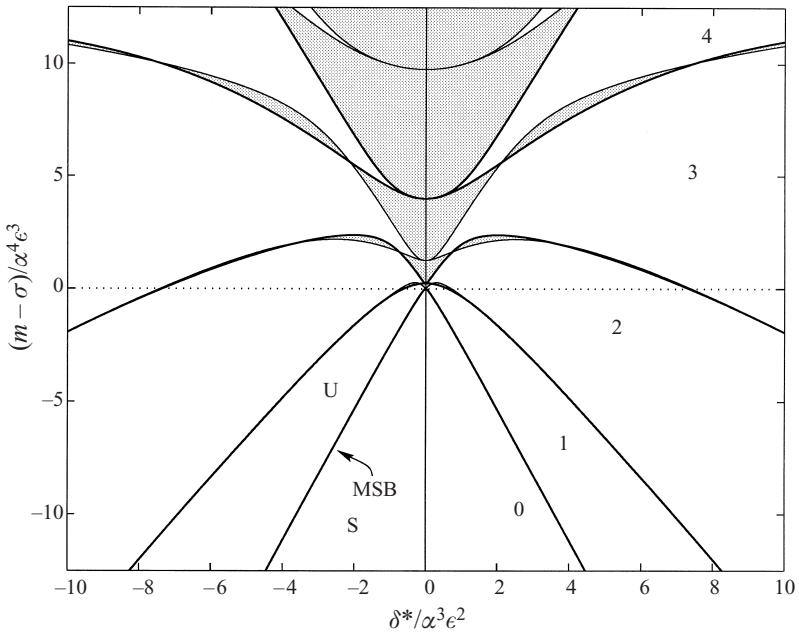


FIGURE 5. Characteristic curves for the longitudinal-roll equation when $\chi = 4.0$. Otherwise the same as figure 4.

morphology has a structure spatially synchronized with the flow. In the longitudinal-roll perturbation, this quantization occurs due to the regularization by the surface tension (cf. equation (5.2)). The morphological cells have secondary structure near the *converging* stagnation points $\alpha\eta = 2n\pi$ (see figure 6). For the two-dimensional disturbance, the quantization occurs at high flow strength (large δ/α^2) beyond the doubly degenerate points. These oscillatory modes are in agreement with the travelling-cell solutions observed in Bühler & Davis (1998), in which left-going cells have localized envelopes at $\alpha\eta = (2n + \frac{1}{2})\pi$, and right-going cells at $\alpha\eta = (2n - \frac{1}{2})\pi$. Superposition of these two solutions leads to cells travelling in the flow direction, with the amplitude confined in narrow envelopes located between the stagnation points (figure 7).

Consider the case when $\sigma = 0$ so that the eigenfunctions are neutrally stable solutions. In the absence of flow, these neutral solutions represents a continuous spectrum along the semi-infinite interval, $m \geqslant 0$. The minimum, $m = 0$, is equivalent to the marginal stability limit of the classical Mullins–Sekerka problem, $M = M_c$ (cf. figure 2*a*). When the flow is present, this continuous spectrum is broken into segments due to parametric resonance, and the eigensolutions that were formerly bounded in the no-flow case now may be amplified. Consequently, sequences of intervals in the parametric space are missing from the spectrum. This scenario is sketched in figure 8, according to the branch-tracing calculations (figures 4 and 5), with the scaled flow strength increasing from figures 8(*a*) to 8(*c*). Bands of the spectrum contract into lines (or extremely thin layers) for a strong flow (figure 8*c*), each of which has a localized structure in space and a quantized morphological number $m^{(v)}$. For the longitudinal rolls, each mode is a solution that has envelopes localized in space and stationary in time, whereas for the two-dimensional cells each mode corresponds to a Hopf bifurcation and consists of a pair of time-dependent, oscillatory solutions.

https://doi.org/10.1017/S0022112099005856 Published online by Cambridge University Press

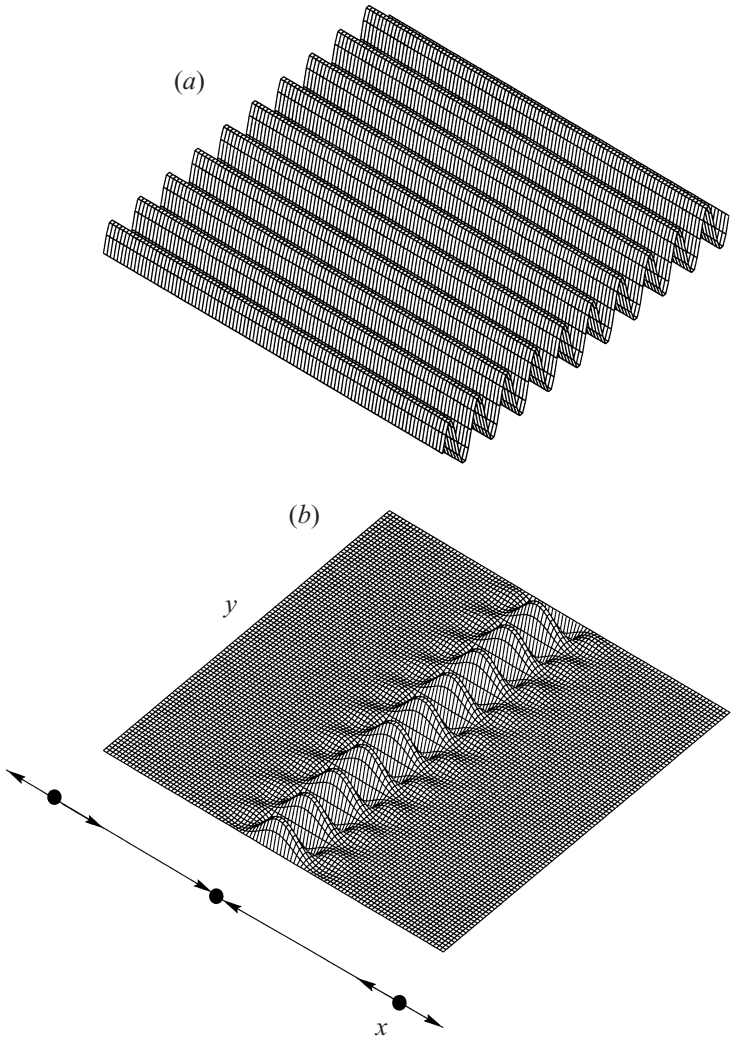


FIGURE 6. Interfacial disturbance of the longitudinal-roll morphology (perspective view) predicted by the linear stability analysis: (*a*) longitudinal rolls in the absence of flow, and (*b*) flow-induced localized morphology. Solid circles are stagnation points and arrows indicate the flow direction.

Consider the stability of the eigensolutions. For given flow and morphological number, the growth rates of the eigenmodes are given by

$$\sigma = m - m^{(v)}, \qquad v = 1, 2, 3, \ldots \ .$$

The unstable modes ($\sigma > 0$) give rise to morphological patterns. If the sequence $\{m^{(v)}\}$ is arranged in an ascending order (cf. figure 8*c*), then the minimum of the spectrum, i.e. $m^{(1)}$, determines the marginal stability limit, since a morphological number $m > m^{(1)}$ leads to modes of positive growth rates and is unstable. This minimum may be viewed as the marginal stability limit 'deformed' from that of the pure morphological problem ($m = 0$) due to the presence of the flow. We shall hereafter refer to this critical value $m^{(1)}$ as m_c, to emphasize that it is the marginal stability limit of the flow-modified morphology.

https://doi.org/10.1017/S0022112099005856 Published online by Cambridge University Press

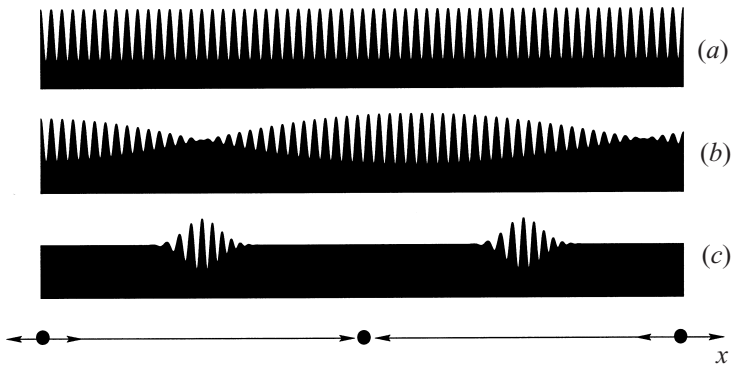


FIGURE 7. Interfacial disturbance of the 2D-roll morphology (side-view) predicted by the linear stability analysis: (*a*) pure, (*b*) incommensurate, and (*c*) localized morphologies. Solid circles are stagnation points and arrows indicate the flow direction.

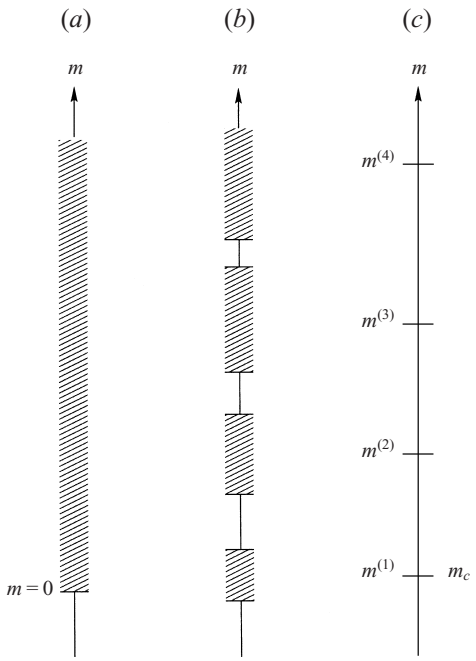


FIGURE 8. Schematics of the flow-perturbed spectrum. Flow strength increases from (*a*) to (*c*).

Our calculations then indicate that the flow stabilizes the two-dimensional disturbance since the marginal morphological number m_c has been delayed ($m_c > 0$), but destabilizes the three-dimensional disturbance because the instability occurs before the pure morphological instability ($m_c < 0$). A WKB-type analysis delivers the asymptotic structures of the quantized modes. The 2D-roll equation is in the form of the one-dimensional Schrödinger equation: $[\partial_\eta^2 + E - U(\eta)]\Psi = 0$, in which the amplitude of the $(2\pi/\alpha)$-periodic potential $U(\eta)$ is equivalent to the flow strength, the energy E corresponds to the morphological number, and the wave function Ψ is analogous to the shape function in our morphological problem. In this case the asymptotic analysis for the second-order, parametric-excitation equation is readily available (e.g. Connor *et al.* 1984). The first eigenmode of the Bohr–Sommerfeld quantization condition

https://doi.org/10.1017/S0022112099005856 Published online by Cambridge University Press

(Fröman 1979) immediately delivers the marginal stability boundaries and the local structures (assuming $\delta > 0$):

$$\left.\begin{aligned} \text{2D-roll:}\quad m_c &\sim \tfrac{1}{2}\alpha\delta^{1/2}, \quad \omega_c \sim \delta - \tfrac{1}{2}\alpha\delta^{1/2}, \\ H &\sim \exp\{\tfrac{1}{4}(-1 \pm \mathrm{i})(\delta/\alpha^2)^{1/2}(\alpha\eta - \alpha\eta_\pm)^2 \pm \mathrm{i}\,\omega_c\tau\}, \quad \delta/\alpha^2 \gg 1. \end{aligned}\right\} \tag{5.3}$$

Here, $\alpha\eta_\pm = (2n \pm \frac{1}{2})\pi$. The requirement that $\hat{\alpha}\hat{\delta}$ in (3.3) should be small sets an upper bound on the validity of the asymptotics. In agreement with the results of the branch-tracing calculations, the eigensolutions have localized structures at the positions where the tangential component of the flow is strong. The discrete modes are the 'turning-point' solutions in the WKB analysis.

For the longitudinal-roll equation, the general theory is not as well-documented as that of the second-order equation, but the structures of the quantized modes can still be obtained from matched asymptotic methods. Through matching the phases of the branches of the WKB solutions, we find that the marginal stability boundary and the localized solution can be approximated by

$$\left.\begin{aligned} \text{longitudinal-roll:}\quad m_c &\sim -(\chi - 1)\alpha\delta^*, \quad \omega_c = 0, \\ H &\sim \int_0^\infty \cos(\xi t)\,\mathrm{e}^{-t^4/4}\,\mathrm{d}t, \quad \delta^*/(\alpha^3\epsilon^2) \gg 1, \end{aligned}\right\} \tag{5.4}$$

where ξ is the distance measured from the centre of the envelope function:

$$\xi = \left(\frac{4\delta^*}{\alpha^3\epsilon^2}\right)^{1/4}(\alpha\eta - 2n\pi). \tag{5.5}$$

One may observe that (5.4) is an eigensolution ($v = 1$ mode) of a 'comparison' equation

$$-\frac{\mathrm{d}^4H}{\mathrm{d}\xi^4} + \xi\frac{\mathrm{d}H}{\mathrm{d}\xi} + vH = 0, \qquad v = 1, 2, 3, \ldots, \tag{5.6}$$

which describes the local behaviour of the parametric-excitation system when the asymptotic expansions $\cos\alpha\eta \sim 1$ and $\sin\alpha\eta \sim \alpha\eta$, and substitutions of (5.5) and $m/(\alpha\delta^*) + \chi = v$ are performed. Integrating (5.6) by the method of steepest descent, we obtain the asymptotic formula for the envelope function:

$$H \sim \sqrt{\tfrac{2}{3}\pi}\,\xi^{-1/3}\exp(-\tfrac{3}{8}\xi^{4/3})\cos(\tfrac{3}{8}\sqrt{3}\xi^{4/3} - \tfrac{1}{6}\pi). \tag{5.7}$$

The above formula is valid in the limit of $1 \ll \xi \ll [\delta^*/(\alpha^3\epsilon^2)]^{1/4}$ or, equivalently, $[\delta^*/(\alpha^3\epsilon^2)]^{-1/4} \ll \alpha\eta \ll 1$ in terms of the flow coordinate.

We can now summarize the morphological instabilities and the related scalings obtained from the linear theory. We see that the imposed spatially periodic flow stabilizes the 2D-roll morphology. The instability is delayed by $(M - M_c) \propto \hat{\alpha}\hat{\delta}^{1/2}$, written in the primitive $\hat{\delta}$–$\hat{\alpha}$ variables. When the rolls have a tilt angle θ the stabilization is then controlled by the factor $\hat{\alpha}(\hat{\delta}\cos\theta)^{1/2}$. Thus, the morphology becomes more unstable as θ approaches $\pi/2$. The most unstable configuration is at $\theta \equiv \pi/2$ (longitudinal rolls), when the above scaling breaks down and the instability moves to $(M - M_c) \propto -\hat{\alpha}\hat{\delta}$. The width of the envelope function changes from $(\hat{\alpha}^2/\hat{\delta})^{1/4}$ for the 2D-roll (cf. equation (5.3)) to $(\hat{\alpha}^3/\hat{\delta})^{1/4}$ for the longitudinal-roll morphology (cf. equation (5.5)).

https://doi.org/10.1017/S0022112099005856 Published online by Cambridge University Press

6. Weakly nonlinear interaction

Near the marginal stability boundary the nonlinear slow-variable equations (4.1), (4.2) may describe evolutions of finite-amplitude disturbances. Of interest is the development of the localized wave envelopes obtained from the linear stability theory. In the asymptotic limits (5.3), (5.4) (cf. figure 8*c*), the discrete, mode-like spectrum is an appropriate setting for bifurcation analysis. Branching solutions at the marginal stability point m_c, and the possible mode–mode interaction nearby can be analysed by the Lyapunov–Schmidt reduction procedure (Golubitsky & Schaeffer 1985). We shall continue considering the two-dimensional and longitudinal versions of the slow-variable dynamics, and focus on the bifurcations of the discrete modes only.

For a given flow, the 2D-roll equation has two oscillatory modes that bifurcate from the homogeneous state. We first shift the coordinate of the singular point m_c and stretch the oscillating frequency ω by imposing the following equations:

$$m = m_c + \lambda, \quad \omega = \omega_c + \varpi(\lambda).$$

The variable λ is viewed as the primary bifurcation parameter. Interactions of the two oscillatory modes near $\lambda = 0$ can be written

$$H(\eta, \tau) = A_1 \mathrm{e}^{\mathrm{i}\omega\tau}\Phi_1(\eta) + A_2 \mathrm{e}^{-\mathrm{i}\omega\tau}\Phi_2(\eta) + W(\eta, \tau).$$

Here, Φ_1 and Φ_2 are the spatial functions of the two eigenmodes, A_i are (complex) modal amplitudes, and W is the perturbed shape function which is set to be orthogonal to Φ_i and is at $o(|A|)$. The reduction procedure projects the nonlinear system (4.1) onto the two-dimensional space (A_1, A_2); the reduced system (bifurcation equation) has the form

$$\left.\begin{aligned} \lambda A_1 - aA_1(\kappa_1|A_1|^2 + \kappa_2|A_2|^2) = 0, \\ \lambda A_2 - aA_2(\kappa_1|A_2|^2 + \kappa_2|A_1|^2) = 0, \end{aligned}\right\} \tag{6.1}$$

in which the coefficients κ_i involve calculations of inner products of Φ_1 and Φ_2.

We compute those coefficients using the asymptotic formula (5.3), and find that $\kappa_1 > 0$ and is $O(1)$, but $\kappa_2 = O([\delta/\alpha^2]^{1/4}\exp[-\tilde{c}(\delta/\alpha^2)^{1/2}])$ where $\tilde{c}$ is a positive $O(1)$ constant. The exponentially small κ_2 results from the fact that the envelopes of the two eigenfunctions (Φ_1 and Φ_2) are separated in space, which results in a weak coupling only. Figure 9(*b*) sketches the bifurcation diagrams showing this mode–mode interaction. It is seen that the mixed-mode, $|A_1| = |A_2| = [\lambda/\{(\kappa_1 + \kappa_2)a\}]^{1/2}$, is stable when $a > 0$ (supercritical), and the pure modes, $|A_i| = [\lambda/(\kappa_1 a)]^{1/2}$, are always unstable. Possible unfolding diagrams through imperfections are exhibited in Golubitsky & Schaeffer (1985).

The longitudinal-roll equation can be analysed by the same procedure. Branches that have the localized structure (5.4) are treated as a single-mode bifurcation, and the equation of the modal amplitude A has the form

$$\lambda A - a\kappa_3 A|A|^2 = 0.$$

Our calculation using (5.4) shows that $\kappa_3 > 0$ and is $O(1)$. The corresponding bifurcation diagram consists of a single pitchfork (figure 9*c*), in which the supercritical branch is stable and subcritical branch unstable.

The fact that κ_1 and κ_3 are $O(1)$, and $\kappa_2 \ll 1$, suggests that, in the scaling regime we have considered, the flow modifies cellular patterns strongly, but the nonlinear branching structures may still be deduced from the pure morphological problem (which determines the sign of a), with the help of symmetry arguments for example.

https://doi.org/10.1017/S0022112099005856 Published online by Cambridge University Press

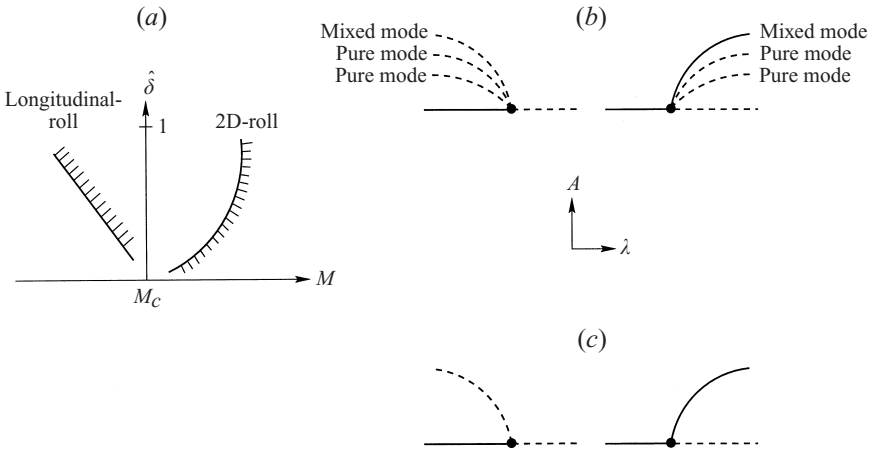


FIGURE 9. Schematics of (*a*) marginal stability boundaries in the asymptotic limits, (*b*) bifurcation diagram for the 2D-roll equation, and (*c*) bifurcation diagram for the longitudinal-roll equation.

It is readily seen that $e^{i\phi}H$ is also a solution if H is a solution of (4.1) or (4.2), where ϕ is an arbitrary phase angle. This $\mathbf{S}^1$ symmetry in a complex plane is due to the translational invariance of the pure morphological cells on the crystal plane. Similarly, $\mathbf{SO}(2) : (A_1, A_2) \rightarrow (e^{i\phi}A_1, e^{-i\phi}A_2)$ due to the translation of time, and $\mathbf{Z}_2 : (A_1, A_2) \rightarrow (A_2, A_1)$ due to reflection in the x-axis, also occur on the travelling cells.

We use numerical computations to verify the bifurcation diagrams obtained above. The slow-variable equations (4.1), (4.2) are integrated using a finite-difference method, with periodic boundary conditions posed on a $2\pi/\alpha$-domain. First, we confirm the stability boundaries and eigenfunction structures predicted by the linear theory. To achieve this purpose we set $a \equiv 0$, and march shape disturbances in time for given pairs of morphological and flow parameters. The number of grid points used here is typically 10^3 in order to resolve the localized structures. Stability boundaries marked by growth or decay of disturbances in long-time evolutions compare favourably with those shown in figures 4 and 5, with deviations of less than 1%.

Next, the structures of bifurcation diagrams, figure 9(*b*, *c*), are verified by examining whether disturbances approach the supercritical solutions when $a > 0$, or are shielded by the barrier of subcritical solutions when $a < 0$. Our computations show that the branching solutions obtained through the reduction procedure are, indeed, realizable. For an example, grey-scale figures 10 and 11 display the evolution of the longitudinal- and 2D-roll dynamics with given parameters. The evolution clearly demonstrates a strong tendency of the flow to produce localized envelopes at the described locations on the interface. The longitudinal rolls are first convected to the converging stagnation point, where the localized envelope forms after a transient time (figure 10). When the interfacial disturbance is reconstructed using the normal mode, the envelope function leads to the cellular pattern shown in figure 6(*b*). For the two-dimensional rolls, disturbances near the stagnation points are suppressed, leaving oscillating wave packets in between (figure 11*a*). This oscillatory pattern is the mixed-mode solution and, when coupled with the roll disturbance $e^{i\beta_c x}$, results in two bands of travelling cells within a flow period (figure 11*b*), as predicted by the linear theory (cf. figure 7c).

https://doi.org/10.1017/S0022112099005856 Published online by Cambridge University Press

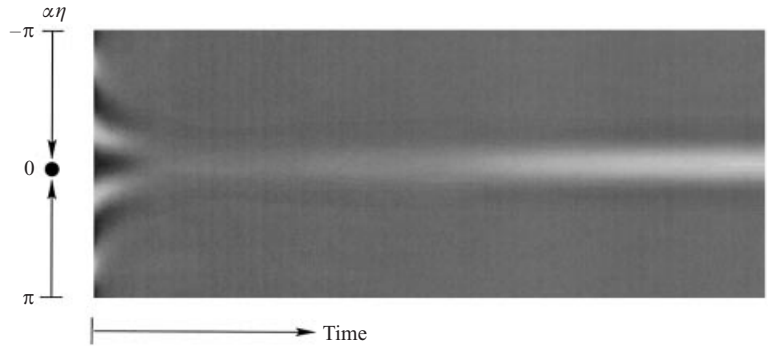


FIGURE 10. Spatiotemporal evolution of a longitudinal-roll disturbance: $\delta^*/(\alpha^3\epsilon^2) = 100$, $m/(\alpha^4\epsilon^2) = -250$, $a/(\alpha^4\epsilon^2) = 6$, and $\chi = 4.0$. Grey-scale represents the height of the interfacial disturbance.

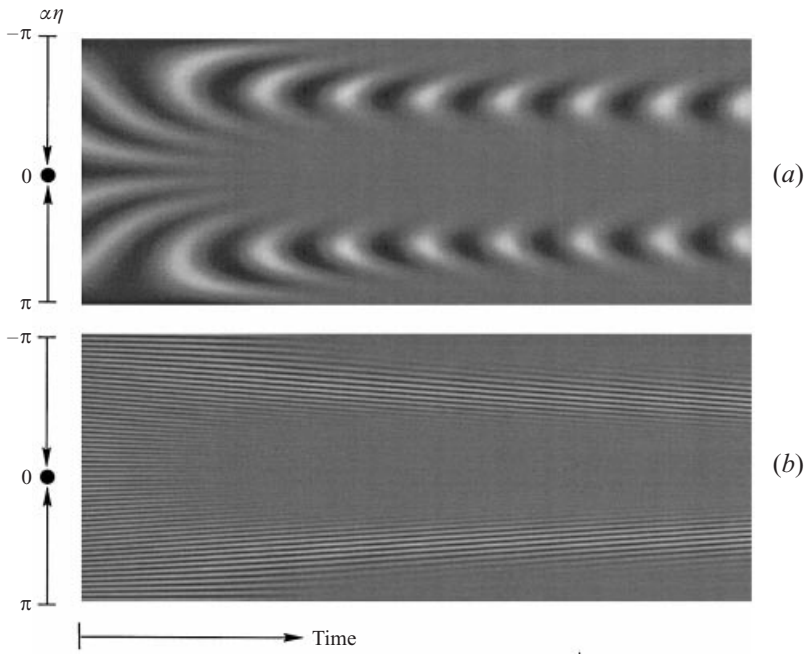


FIGURE 11. Spatiotemporal evolution of (*a*) a 2D-roll disturbance: $\delta/\alpha^2 = 400$, $m/\alpha^2 = 13$, $a/\alpha^2 = 6$, and (*b*) the corresponding two-dimensional travelling cells. Grey-scale represents the height of the interfacial disturbance.

7. Conclusions

In summary, we investigated the effects of a cellular convective flow imposed on the directional solidification of a dilute binary alloy. The imposed flow has spatial wavenumber $\hat{\alpha}$ and strength parameter $\hat{\delta}$ that control the perturbation to the interfacial deformation. A multiple-scale analysis is performed near the onset of the morphological instability, which results in a weakly nonlinear equation in slow space–time variables. The dynamics of the front is parametrically excited by the imposed flow. Its linear problem is solved by the numerical branch-tracing method. We find that the remote, spatially periodic flow stabilizes two-dimensional disturbances in the

https://doi.org/10.1017/S0022112099005856 Published online by Cambridge University Press

flow direction, yet promotes three-dimensional instability. The previously observed, localized two-dimensional morphology (Bühler & Davis 1998) is identified as the quantization of the eigenstates, in which the unstable modes are discrete in an unbounded space, and the perturbed interfacial structures are forced to be spatially synchronized with the flow. The stability boundary and the asymptotic structure of the eigenmodes are obtained by the WKB method in the limit of $\hat{\alpha} \to 0$. The nonlinear branching structure is delivered through the Lyapunov–Schmidt procedure. Numerical computations confirm the analytical results.

Linear stability analysis shows that the flow stabilizes two-dimensional but destabilizes three-dimensional disturbances. The mechanism may be tightly bound with the structure of the neutral stability curve shown in figure 2(*a*). A disturbance along the flow direction (figure 7) is either compressed or stretched near the stagnation points by the tangential-flow component. This effectively changes its wavenumber so that the local β becomes larger or smaller than the critical value of the pure morphological instability. The surface tension or solute diffusion help stabilize the interface locally. In contrast, when a disturbance has a three-dimensional structure (figure 6), the solute redistribution will play an important role. The imposed convective field raises the solute concentration at the converging stagnation points (cf. equation (3.4)) and promotes the constitutional undercooling. This redistribution is further amplified by the normal component near the perturbed interface, which lowers the critical morphological number and hence destabilizes the interface. The two mechanisms then suggest that, near the onset of the instability, patterns like figure 7 may occur in a confined, two-dimensional geometry (Hele-Shaw slot, for example). In a fully three-dimensional setting one would expect to see a pattern close to figure 6, since it is preferred. We note that qualitatively similar behaviour has been reported in the earlier experiment of Hämäläinen (1967), who found that morphological instability occurs first at convergent stagnation points that are at the corners of convection cells in a three-dimensional setting, even though in his experiment the flow and morphological cells have comparable wavelengths.

This work was supported by NASA, Microgravity Sciences and Application Programs.

REFERENCES

Brattkus, K. & Davis, S. H. 1988 *J. Cryst. Growth* **89**, 423.
Bühler, L. & Davis, S. H. 1988 *J. Cryst. Growth* **186**, 629.
Connor, J. N. L., Uzer, T., Marcus, R. A. & Smith, A. D. 1984 *J. Chem. Phys.* **80**, 5095.
Coriell, S. R., Cordes, M. R., Boettinger, W. S. & Sekerka, R. F. 1980 *J. Cryst. Growth* **49**, 13.
Coriell, S. R. & McFadden, G. B. 1989 *J. Cryst. Growth* **94**, 513.
Coriell, S. R., McFadden, G. B. & Boisvert, R. F. 1984 *J. Cryst. Growth* **69**, 15.
Davis, S. H. 1993 In *Handbook of Crystal Growth* (ed. D. T. J. Hurle), Vol. 1, Ch. 13, p. 861. Elsevier Science Publishers.
Doedel, E. J. 1981 *Congressus Numerantum* **30**, 265.
Forth, S. A. & Wheeler, A. A. 1989 *J. Fluid Mech.* **202**, 339.
Fröman, N. 1979 *J. Phys.* A **12**, 2355.
Golubitsky, M. & Schaeffer, D. 1985 *Singularities and Groups in Bifurcation Theory*. Springer.
Hämäläinen, M. 1967 *J. Cryst. Growth* **1**, 125.
Hobbs, A. K. & Metzener, P. 1991 *J. Cryst. Growth* **112**, 539.
Langer, J. S. 1980 *Rev. Mod. Phys.* **52**, 1.
McLachlan, N. W. 1947 *Theory and Application of Mathieu Functions*. Clarendon.

https://doi.org/10.1017/S0022112099005856 Published online by Cambridge University Press

Mulholland, H. P. & Goldstein, S. 1929 *Phil. Mag.* **8**, 834.
Mullins, W. W. & Sekerka, R. F. 1964 *J. Appl. Phys.* **35**, 444.
Newell, A. C. & Whitehead, J. A. 1969 *J. Fluid Mech.* **38**, 279.
Pal, D. & Kelly, R. E. 1979 *ASME Paper* 79-HT-109.
Schulze, T. P. & Davis, S. H. 1994 *J. Cryst. Growth* **143**, 317.
Walton, I. C. 1982 *Q. J. Mech. Appl. Maths* **35**, 33.
Wollkind, D. J. & Segel, L. A. 1970 *Phil. Trans. R. Soc. Lond.* A **268**, 351.

https://doi.org/10.1017/S0022112099005856 Published online by Cambridge University Press